



Semnan University

# Mechanics of Advanced Composite Structures

journal homepage: <http://MACS.journals.semnan.ac.ir>

## Free Natural Frequency Analysis of an FG Composite Rectangular Plate Coupled with Fluid using Rayleigh–Ritz Method

K. Khorshidi\*, A. Bakhsheshy

Sound and Vibration Laboratory, Department of Mechanical Engineering, Faculty of Engineering, Arak University, Arak, 38156-88349, Iran.

### PAPER INFO

#### Paper history:

Received 7 August 2014

Received in revised form 1 November 2014

Accepted 11 November 2014

#### Keywords:

Rectangular plates

Vibration

Analytical modelling

FG composite

Sloshing fluid

### ABSTRACT

This study investigates natural frequency analysis of an FG composite rectangular plate partially contacting with a bounded fluid. The material properties are assumed to be varying continuously through the thickness direction according to a simple power law distribution in terms of volume fraction of material constituents. Wet dynamic transverse displacements of the plate are approximated by a set of admissible trial functions which are required to satisfy the clamped and simply supported geometric boundary conditions. Fluid velocity potential satisfying fluid boundary conditions is derived and wet dynamic modal functions of the plate are expanded in terms of finite Fourier series for compatibility requirement along the contacting surface between the plate and the fluid. Natural frequencies of the plate coupled with sloshing fluid modes are calculated using Rayleigh–Ritz method based on minimizing the Rayleigh quotient. The proposed analytical method is validated by available data in the literature. The numerical results show the effects of boundary conditions, aspect ratios, thickness ratios, gradient index, material properties of the FG plate, depth of the fluid and dimensions of the tank on the wet natural frequencies.

© 2014 Published by Semnan University Press. All rights reserved.

## 1. Introduction

Functionally Graded Materials (FGMs) have been developing rapidly in the past two decades. Nowadays FGMs are used widely in many engineering applications including aircraft and aerospace industry, micro and nano electromechanical system, thermal barrier coating etc. Numerous studies have been performed to investigate free and forced vibrations of thin isotropic plates in partial contact with a fluid. Some of the most complete reviews on the subject are presented by Khorshidi [1], Amabili [2], Jeong et al. [3-5], Kwak [6], Zhou and Cheung [7], Chang and Liu [8], Ergin and Uğurlu [9], Zhou and Liu [10], Uğurlu et al. [11], and Kerboua et al. [12].

A few researchers have employed Classical Plate Theory (CPT) to analyze vibration behaviour of thin FG plates (Abrate [13], Zhang and Zhou [14] and Woo et al. [15]). First and third order shear deformation plate theory and three-dimensional elasticity theory are used by some investigators for analyzing thick FG plates. Early research efforts on harmonic vibration analysis of an FG simply-supported rectangular plate, using a 3D asymptotic theory, date back to the work of Reddy and Cheng [16]. Qian et al. [17] conducted an investigation on free and forced vibrations and static deformations of an FG thick simply-supported square plate by using a higher-order shear and normal deformable plate theory and a meshless local Petrov–Galerkin method. Vel and Batra [18] did an excellent investigation on the analytical solution for free and forced vibrations of FG

\* Corresponding author. Tel. +98-86-32625720; Fax: +98-86-34173450

E-mail address: k-khorshidi@araku.ac.ir

simply-supported square plates based on the 3D elasticity solution. Hosseini-Hashemi et al. presented analytical solutions for free vibration analysis of FGMs rectangular plates based on the First-order Shear Deformation Plate Theory (FSDT) [19] and Third-order Shear Deformation Theory (TSDT) [20]. In their study, the proposed rectangular plates have two opposite edges simply-supported, while all possible combinations of free, simply-supported and clamped boundary conditions are applied to the other two edges. Suresh Kumar et al. [21] develop an analytical solution to study the free vibration analysis of FGM plate without enforcing zero transverse shear stress conditions on the top and bottom surfaces of the plate using higher order displacement model. In their study, the governing equations of FGM plate are established using energy principles and are solved using Navier's method. Jha et al. [22] presented free vibration analysis of FG elastic, rectangular, and simply supported (diaphragm) plates using a Higher Order Shear and Normal Deformation Theory (HOSNT). Jha et al. assumed the material properties of FG plates to be varying through thickness of the plate in a continuous manner. They used Navier solution method to solve the equations of motion. Zhao et al. [23] present free vibration analysis of metal and ceramic FG plates based on FSDT using the element-free kp-Ritz method. The material properties of the plates are assumed to vary continuously through their thickness according to a power-law distribution of the volume fractions of the plate constituents. The mesh-free kernel particle functions are used to approximate the two dimensional displacement fields. Four types of FG rectangular and skew plates of Al/Al<sub>2</sub>O<sub>3</sub>, Al/ZrO<sub>2</sub>, Ti-6Al-4V/Aluminum oxide, and SUS304/ Si<sub>3</sub>N<sub>4</sub> are included in their study. Huang et al. [24] reported an accurate solution of the free vibration characteristics of side-cracked rectangular FGM thick plates. Huu et al. [25] developed a refined shear deformation theory for free vibration of FG plates on elastic foundation. Zhu and Liew [26] presented free vibration analyses of metal and ceramic FG plates with the local Kriging meshless method based on the FSDT and the local Petrov-Galerkin formulation.

The governing equations and a detailed analysis of vibrating rectangular plates in contact with a fluid can be found in Khorshidi [1], Khorshidi and Farhadi [27], and Jeong [3-5] works. Such equations are not available for FG plates in the literature. Compensating for this apparent void, the present work is carried out to provide a theory to calculate the wet natural frequencies of an FG rectangular plate partially contacting with a bounded fluid in the bottom and vertical direction using Rayleigh-Ritz method. In the developed model, the von Kàrmàn linear strain-

displacement relationships are used in order to obtain kinetic and strain energies of the plate based on CPT, FSDT and TSDT. The contributions given by the presence of the fluid and by the sloshing effects of the free surface are also included in the model. In conclusion, the results show that the fluid in contact with the plate changes the linear dynamics completely. Therefore, fluid-structure interaction is carefully considered. The developed numerical models are able to reproduce such results with good accuracy. Finally, the effects of boundary conditions, aspect ratio, thickness ratio, gradient index, material properties of the FG plate, depth of the fluid and dimensions of the tank on the wet natural frequencies are investigated.

## 2. Elastic Strain and Kinetic Energies of an FG Plate

An FG composite rectangular plate with length  $a$ , width  $b$ , thickness  $h$ , which is a part of the vertical side of a bounded rigid tank filled with a fluid, is considered as shown in Fig. 1. The tank has width of  $c_1$  and the fluid is of depth  $b_1$  and mass density of  $\rho_F$ . The fluid is considered to be incompressible, inviscid and irrotational. A Cartesian coordinate system is used to describe governing equations. The coordinate system is placed so that the origin is located in the corner of the studied plate as shown in Fig. 1, while axes  $x$  and  $y$  lie on plate's edges and axis  $z$  is perpendicular to the middle plane. The boundary conditions of the plate are introduced in Appendix A.

We Assume that in FGM the material composition varies smoothly from the top surface ( $z=0$ ) to the bottom surface ( $z=-h$ ) of the plate (in this study, the FG plate is made from a mixture of ceramics and

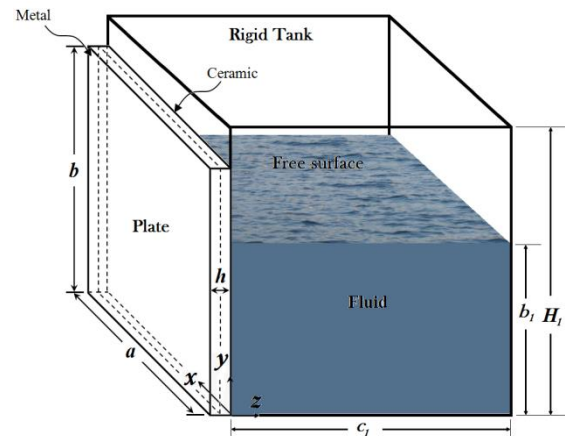


**Figure 1.** FGM composite rectangular plate in contact with liquid, dimensions, coordinates and displacement systems

metal). In this case, the effective mechanical properties of the plate, such as Young's modulus and density, are assumed to vary continuously through the plate thickness according to a power-law distribution as the following:

$$E(z) = (E_m - E_c) \mathcal{V}_m + E_c \tag{1}$$

$$\rho(z) = (\rho_m - \rho_c) \mathcal{V}_m + \rho_c \tag{2}$$

where the subscripts *m* and *c* represent the metallic and ceramic constituents, respectively, and the volume fraction  $\mathcal{V}_m$  may be given by:

$$\mathcal{V}_m = \left(\frac{-z}{h}\right)^\alpha \tag{3}$$

where  $\alpha$  is the gradient index and takes only positive values. Fig. 2 shows the variation of Young's modulus through the dimensionless thickness for the FGM Al/ZrO2 plate. The top surface is ceramic rich and the bottom surface is metal rich. Typical values for metal and ceramics used in the FG plate are listed in Table 1.

The stress-strain relations for the FG rectangular plates, under the hypothesis  $\sigma_z = 0$ , in the material principal coordinates, are given by:

**Table 1.** Material properties of the Functionally Graded plates [19] and [20].

Material	properties	
	<i>E</i> (GPa)	$\rho$ (kg/m <sup>3</sup> )
Al	70	2702
Ti-6Al-4V	105.7	4429
AL <sub>2</sub> O <sub>3</sub>	380	3800
ZrO <sub>2</sub>	200	5700
Aluminum Oxide	320.2	3750

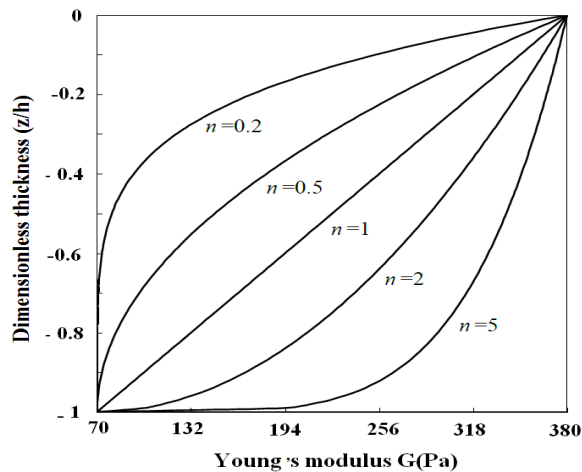


**Figure 2.** Variation of Young's modulus through the dimensionless thickness of Al/ZrO2 plate.

$$\begin{pmatrix} \sigma_x \\ \sigma_y \\ \sigma_{xy} \\ \sigma_{xz} \\ \sigma_{yz} \end{pmatrix} = \begin{bmatrix} Q_{11} & Q_{12} & 0 & 0 & 0 \\ Q_{12} & Q_{11} & 0 & 0 & 0 \\ 0 & 0 & Q_{33} & 0 & 0 \\ 0 & 0 & 0 & Q_{33} & 0 \\ 0 & 0 & 0 & 0 & Q_{33} \end{bmatrix} \begin{pmatrix} \varepsilon_x \\ \varepsilon_y \\ \varepsilon_{xy} \\ \varepsilon_{xz} \\ \varepsilon_{yz} \end{pmatrix} \tag{4}$$

Where  $Q_{11} = E(z)/1 - \nu^2$ ,  $Q_{12} = \nu Q_{11}$  and  $Q_{33} = E(z)/2(1 + \nu)$ ,  $\varepsilon_x$ ,  $\varepsilon_y$ ,  $\varepsilon_{xy}$ ,  $\varepsilon_{xz}$  and  $\varepsilon_{yz}$  are the strain components (see Appendix B), and  $\nu$  is the Poisson's ratio of the plate. The elastic strain energy  $U_P$  of the plate is given by:

$$U_P = \frac{1}{2} \int_0^a \int_0^b \int_{-h}^0 (\sigma_x \varepsilon_x + \sigma_y \varepsilon_y + \sigma_{xy} \varepsilon_{xy} + K_x^2 \sigma_{xz} \varepsilon_{xz} + K_y^2 \sigma_{yz} \varepsilon_{yz}) dz dy dx \tag{5}$$

where  $K_x$  and  $K_y$  are the shear correction factors, which are equal to one (no correction) for the third-order shear deformation theory. The shear correction factor used in the present calculations (for the first-order shear deformation theory) is  $K_x^2 = K_y^2 = \sqrt{3}/2$  [27]. The kinetic energy  $T_P$  of the plate, including rotary inertia, is given by:

$$T_P = \frac{1}{2} \int_0^a \int_0^b \int_{-h}^0 \rho(z) [\dot{u}_1^2 + \dot{u}_2^2 + \dot{u}_3^2] dz dy dx \tag{6}$$

where the overdot denotes time derivative. The boundary conditions on bending moments for clamped boundary condition of the plates can be approximated by assuming that rotational springs of very high stiffness  $\kappa$  are distributed along the plate edges, so an additional potential energy stored by the elastic rotational springs at the plate edges must be added. This potential energy  $U_R$  is given by:

$$U_R = \frac{1}{2} \int_0^b \kappa \left\{ \left[ \left( \frac{\partial w}{\partial x} \right)_{x=0} \right]^2 + \left[ \left( \frac{\partial w}{\partial x} \right)_{x=a} \right]^2 \right\} dy + \frac{1}{2} \int_0^a \kappa \left\{ \left[ \left( \frac{\partial w}{\partial x} \right)_{y=0} \right]^2 + \left[ \left( \frac{\partial w}{\partial x} \right)_{y=b} \right]^2 \right\} dx \tag{7}$$

In order to simulate clamped edges in numerical calculations, a very high value of the stiffness ( $\kappa \rightarrow \infty$ ) must be assumed. This approach is usually referred to as the artificial spring method, which can be regarded as a variant of the classical penalty method. The values of the spring stiffness simulating a clamped plate can be obtained by studying the convergence of the natural frequencies of the linearized solution by increasing the value of  $\kappa$ . In fact, it is found that the natural frequencies of the system converge asymptotically with those of a clamped

plate when  $\kappa$  becomes very large (in this study the non-uniform stiffness is assumed as  $\kappa = 10^8$ ) [27].

### 3. Formulation of the Fluid Oscillations

Using the principle of superposition, the fluid velocity potential  $\Phi_O$ , can be obtained as follows:

$$\Phi_O = \Phi_B + \Phi_S \quad (8)$$

where  $\Phi_B$  describes the velocity potential of the fluid obtained by neglecting free surface waves and  $\Phi_S$  is the velocity potential due to fluid sloshing in the presence of the rigid plate. The fluid velocity potential can be separated into spatial velocity potential and a harmonic time function.

$$\Phi_O(x, y, z, t) = \phi_O(x, y, z) \exp(i \omega t) \quad (9)$$

The fluid velocity potential must satisfy the three dimensional Laplace equation in the fluid domain.

$$\nabla^2 \phi_O = \nabla^2 \phi_B + \nabla^2 \phi_S = 0 \quad (10)$$

The boundary conditions on the bottom and the vertical walls of the tank are given by:

$$\begin{aligned} \frac{\partial \phi_B}{\partial x} \Big|_{x=0} = \frac{\partial \phi_B}{\partial x} \Big|_{x=a} = 0, \quad \frac{\partial \phi_B}{\partial y} \Big|_{y=0} = 0 \\ \frac{\partial \phi_B}{\partial z} \Big|_{z=c_1} = 0, \quad \frac{\partial \phi_S}{\partial x} \Big|_{x=0} = \frac{\partial \phi_S}{\partial x} \Big|_{x=a} = 0 \\ \frac{\partial \phi_S}{\partial y} \Big|_{y=0} = 0, \quad \frac{\partial \phi_S}{\partial z} \Big|_{z=0, c_1} = 0 \end{aligned} \quad (11-18)$$

For the liquid upper surface with neglecting of the liquid sloshing, we obtain the following equation:

$$\phi_B \Big|_{y=b_1} = 0 \quad (19)$$

For the liquid-contacting surface of the elastic plate, the following equation is obtained:

$$\frac{\partial \Phi_B}{\partial z} \Big|_{z=0} = \frac{\partial w(x, y, t)}{\partial t} \quad (20)$$

where  $w(x, y, t)$  is the transverse deflection of the plate. Applying the method of separating variables based on the boundary conditions of Eqs. (11-19), general solution of Eq. (10) is given as follows:

$$\begin{aligned} \Phi_B(x, y, z, t) = \sum_{l=0}^{\infty} \sum_{k=0}^{\infty} A_{l,k}(t) \cos\left(\frac{l\pi x}{a}\right) \times \\ \cos\left(\frac{(2k+1)\pi y}{2b_1}\right) \left\{ e^{\sigma z} + e^{\sigma(2c_1-z)} \right\} \\ 0 \leq x \leq a, 0 \leq y \leq b_1, 0 \leq z \leq c_1 \end{aligned} \quad (21)$$

$$\begin{aligned} \Phi_S(x, y, z, t) = \sum_{i=0}^{\infty} \sum_{j=0}^{\infty} B_{i,j}(t) \cos\left(\frac{i\pi x}{a}\right) \times \\ \cosh(\tau y) \cos\left(\frac{j\pi z}{c_1}\right) \\ (0 \leq x \leq a), (0 \leq y \leq b_1), (0 \leq z \leq c_1) \end{aligned} \quad (22)$$

where  $\sigma = \pi \sqrt{(l/a)^2 + ((2k+1)/(2b_1))^2}$ , here  $l$  and  $k$  are arbitrary nonnegative integers,  $\tau = \pi \sqrt{(i/a)^2 + (j/c_1)^2}$ , here  $i$  and  $j$  are arbitrary nonnegative integers, and  $A_{l,k}(t)$  and  $B_{i,j}(t)$  are the unknown coefficients. Applying the compatibility condition of Eq. (20), one obtains the following [27]:

$$\begin{aligned} A_{l,k}(t) = \frac{coeff_1}{ab_1} \int_0^a \int_0^{b_1} w(x, y, t) \cos\left(\frac{l\pi x}{a}\right) \times \\ \cos\left(\frac{(2k+1)\pi y}{2b_1}\right) dy dx / (\sigma \{1 - \exp(2c_1\sigma)\}) \\ coeff_1 = \begin{cases} (1 \text{ if } l \text{ and } k = 0), \\ (2 \text{ if } l \text{ or } k = 0), \\ (4 \text{ if } l, k \neq 0) \end{cases} \end{aligned} \quad (23)$$

By the assumption of the ideal fluid and no surface waves, the kinetic energy of the fluid with respect to the bulging modes of the plate and the fluid sloshing can be written as follows[27]:

$$T_{fB} = \frac{1}{2} \rho_F \int_0^a \int_0^{b_1} \Phi_B \Big|_{z=0} \left( -\frac{\partial w}{\partial t} \right) dy dx \quad (24)$$

$$T_{fS} = \frac{1}{2} \rho_F \int_0^a \int_0^{b_1} \Phi_S \Big|_{z=0} \left( -\frac{\partial w}{\partial t} \right) dy dx \quad (25)$$

The linearized sloshing conditions at the fluid free surface of the tank are as the following:

$$\frac{\partial \Phi_O}{\partial y} \Big|_{y=b_1} = \frac{\omega^2}{g} \Phi_O \Big|_{y=b_1} \quad (26)$$

where  $g$  is the gravity acceleration and  $\omega$  is the circular natural frequency of the liquid-coupled plate.

Substituting Eq. (8) with Eq. (26) and using Eq. (19), one obtains the following:

$$\frac{\partial \Phi_B}{\partial y} \Big|_{y=b_1} + \frac{\partial \Phi_S}{\partial y} \Big|_{y=b_1} = \frac{\omega^2}{g} \Phi_S \Big|_{y=b_1} \quad (27)$$

Multiplying both sides of the Eq. (27) by  $\rho_F \Phi_S$  then integrating them over the free surface of the fluid in the tank lead to the following equation:

$$U_{\phi_B} + U_{\phi_S} = \omega^2 T_{\phi_S}, \quad (28)$$

where:

$$U_{\phi_B} = \rho_F \int_0^a \int_0^{c_1} \left( \Phi_S \frac{\partial \Phi_B}{\partial y} \right)_{y=b_1} dz dx \quad (29)$$

$$U_{\phi_S} = \rho_F \int_0^a \int_0^{c_1} \left( \Phi_S \frac{\partial \Phi_S}{\partial y} \right)_{y=b_1} dz dx \quad (30)$$

$$T_{\phi_S} = \frac{\rho_F}{g} \int_0^a \int_0^{c_1} \left( \Phi_S^2 \right)_{y=b_1} dz dx \quad (31)$$

#### 4. Rayleigh–Ritz Approach

The Lagrangian function of the fluid-plate coupled system is as follows:

$$\Pi = \sum_{\max} Starin E. - \sum_{\max} Kinetic E. \quad (32)$$

With applying Ritz minimization method, an eigenvalue equation can be derived from Eq. (32) as the following:

$$\frac{\partial \Pi}{\partial q} = 0, \quad (33)$$

where  $q$  is the vector of generalized coordinates and contains the unknown time variable coefficients of the admissible trial functions presented by Eqs. (B 26-40) and (22) (i.e.

$q = \{u_{m,n}, v_{m,n}, w_{m,n}, \phi_{1m,n}, \phi_{2m,n}, B_{i,j}\}^T$ ). Following minimization the Eq. (33), the subsequent equation is obtained:

$$\left( K_p + K_R \right) C_{m,n} - \omega^2 \left[ \left( M_p + M_{fB} \right) C_{m,n} + M_{fS} B_{i,j} \right] = 0, \quad (34)$$

where  $C_{m,n} = \{u_{m,n}, v_{m,n}, w_{m,n}, \phi_{1m,n}, \phi_{2m,n}\}^T$  and

$$K_p = \frac{\partial^2 U_p}{\partial q_i \partial q_j} \quad (35)$$

$$K_R = \frac{\partial^2 U_R}{\partial q_i \partial q_j} \quad (36)$$

$$M_p = \frac{\partial^2 T_p}{\partial q_i \partial q_j} \quad (37)$$

$$M_{fB} = \frac{\partial^2 T_{fB}}{\partial q_i \partial q_j} \quad (38)$$

$$M_{fS} = \frac{\partial^2 T_{fS}}{\partial q_i \partial q_j} \quad (39)$$

Eq. (34) cannot be solved until an expression for  $B_{i,j}$  is obtained. Thus, Eq. (28) is added to the Galerkin equation (34). This act increases the dimensions of the associated eigenvalue problem from  $(\bar{N} \times \bar{N})$  to  $((\bar{N} + \tilde{N}) \times (\bar{N} + \tilde{N}))$  where  $\bar{N}$  is the dimension of the coordinates vector  $q = \{w_{m,n}\}^T$  and  $\tilde{N}$  is the dimension of coordinates vector  $q = \text{tor } q = \{B_{i,j}\}^T$ . Consequently, the following Galerkin equation is obtained:

$$\begin{bmatrix} K_p + K_R & 0 \\ K_{\phi_B} & K_{\phi_S} \end{bmatrix} \begin{Bmatrix} C_{m,n} \\ B_{i,j} \end{Bmatrix} - \omega^2 \begin{bmatrix} M_p + M_{fB} & M_{fS} \\ 0 & M_{\phi_S} \end{bmatrix} \begin{Bmatrix} C_{m,n} \\ B_{i,j} \end{Bmatrix} = 0 \quad (40)$$

where

$$K_{\phi_B} = \frac{\partial^2 U_{\phi_B}}{\partial q_i \partial q_j} \quad (41)$$

$$K_{\phi_S} = \frac{\partial^2 U_{\phi_S}}{\partial q_i \partial q_j} \quad (42)$$

$$M_{\phi_S} = \frac{\partial^2 T_{\phi_S}}{\partial q_i \partial q_j} \quad (43)$$

#### 5. Comparative Study

In order to validate the present formulation, the natural frequencies obtained by the present method are compared with those of Bishop (1979), Zhao et al. (2009), Hosseini-Hashemi et al. (2010) and Uğurlu et al. (2008), as listed in Tables 2-5. Calculations are performed for functionally graded rectangular plates. Material properties of the plate are defined as listed in Table 1. Also, fluid density is considered as  $\rho_F = 1000 \text{ kg / m}^3$ .

Table 2 shows a comparative study of the natural frequencies of simply supported FG square plates with those given by Bishop (1979), Zhao et al. (2009). The geometric properties of the plates are  $a = b = 0.4\text{m}$  and  $h = 0.005\text{m}$ . The material properties of the Aluminum oxide/Ti-6Al-4V are listed in Table 1. The results shown in this table are selected for two special gradient index components  $\alpha = 0$  (Pure Metal) and  $\alpha = 2000$  (Pure Ceramic). It is seen that the solutions from this study agree well with those presented by Bishop and Zhao et al. In Tables 3 and 4, the fundamental non-dimensional natural frequencies ( $\beta = \omega b^2 / h \sqrt{\rho_c / E_c}, \omega(\text{Hz})$ ) of a simply supported functionally graded square plate are compared with those reported by Zhao et al. (2009), and Hosseini-Hashemi et al. (2010) for different gradient indexes. It is worth noting that the results of Tables 3 and 4 are calculated for square (AL/Al<sub>2</sub>O<sub>3</sub>) material. In these tables the fundamen-

tal non-dimensional natural frequencies of the simply supported functionally graded plate are computed using the Classical Plate Theory (CPT), the First order Shear Deformation Plate Theory (FSDT) and the Third order Shear Deformation Plate Theory (TSDT). From the results presented in these tables, it is observed that the non-dimensional natural frequencies decrease as the gradient index increases. In addition, the fundamental natural frequencies computed CPT are not at the same accuracy of those provided FSDT and TSDT.

In Table 5, the fundamental non-dimensional natural frequencies ( $\beta = \alpha a^2 \sqrt{\rho_f h / D}, \omega(\text{Hz})$ ) of a simply supported square isotropic plate in partial contact with water are reported for different fluid depth ratios including  $b_1 / b = 0, 0.2, 0.4, 0.6, 0.8,$  and  $1$ . The results are compared with those obtained by Uğurlu et al. (2008) based on the CPT. In this table calculations are performed for a square plate with dimensions and material properties of  $a = 10\text{m}, b = 10\text{m}, h = 0.15\text{m}, \rho = 2400\text{ kg/m}^3, E = 25\text{ GPa}$  and  $\nu = 0.15$ , and width of the tank is  $c_1 = 100\text{m}$ . It is worth mentioning that Uğurlu et al. calculate their results for a rectangular plate in contact with an infinite fluid ( $c_1 = \infty$ ).

It is observed from Table 5 that the fundamental natural frequency of the plate increases monotonically, as the fluid depth ratio tends to zero. It is also observed that the mode sequence changes according to the fluid depth. Table 5 shows that there is a good agreement between the present results and those of Uğurlu et al. (2008).

From Tables 2-5, it is observed that the accuracy of fundamental natural frequencies computed by CPT decreases as the thickness ratio increases.

### 6. Numerical Results and Discussion

In this section, numerical results are obtained according to the developed analytical solution for the free vibrations of a functionally graded rectangular plate in air or in contact with the bounded fluid by

**Table 2.** Comparison of the fundamental natural frequency (Hz) for simply supported square Ti-Al-4V/Aluminum Oxide Functionally Graded plates ( $a=b = 0.4\text{m}, h = 0.005\text{m}$ ).

Mode Sequence	Pure Metal, $\alpha = 0$				
	Present (CPT)	Present (FSDT)	Present (TSDT)	Ref [23]	Ref [28]
1	145.021	144.968	144.958	143.67	145.04
2	362.484	362.153	362.087	360.64	362.61
3	362.484	362.153	362.087	360.64	362.61
4	579.862	579.017	578.848	575.87	580.18
5	724.735	723.415	723.152	725.53	725.22
6	724.735	723.415	723.152	725.53	725.22
7	941.974	939.748	939.304	938.18	942.79
8	941.974	939.748	939.304	938.18	942.79
9	1231.5	1227.7	1226.94	1238.76	1233.0
10	1231.5	1227.7	1226.94	1238.76	1233.0

Mode Sequence	Pure Ceramic, $\alpha \rightarrow \infty$				
	Present (CPT)	Present (FSDT)	Present (TSDT)	Ref [23]	Ref [28]
1	271.174	270.975	271.061	268.60	271.23
2	677.803	676.567	677.099	674.38	678.06
3	677.803	676.567	677.099	674.38	678.06
4	1084.28	1081.12	1082.48	1076.8	1084.9
5	1355.17	1350.25	1352.36	1356.9	1356.1
6	1355.17	1350.25	1352.36	1356.9	1356.1
7	1761.38	1753.09	1756.65	1754.4	1763.0
8	1761.38	1753.09	1756.65	1754.4	1763.0
9	2302.76	2288.63	2294.68	2316.9	2305.4
10	2302.76	2288.63	2294.68	2316.9	2305.4

**Table 3.** Comparison of the fundamental natural frequency parameter  $\beta = (\omega b^2 / h) \sqrt{\rho_c / E_c}, \omega(\text{Hz})$  for simply supported Al/Al<sub>2</sub>O<sub>3</sub> Functionally Graded square plates ( $a/b = 1, h/a=0.05$ ).

$\alpha$	Present (CPT)	Present (FSDT)	Present (TSDT)	Ref [19]	Ref [23]	Diff
						with [19] (TSDT)
0	0.01490	0.01482	0.01480	0.01480	0.01464	0
0.5	0.01262	0.01256	0.01254	0.01281	0.01241	0.21
1	0.01137	0.01132	0.01131	0.01150	0.01118	1.67
4	0.00988	0.00983	0.00980	0.01013	0.00970	3.36
10	0.00950	0.00943	0.00941	0.00963	0.00931	2.33

**Table 4.** Comparison of the fundamental natural frequency parameter  $\beta = (\omega b^2 / h) \sqrt{\rho_c / E_c}$ ,  $\omega$ (Hz) for simply supported Al/Al<sub>2</sub>O<sub>3</sub> functionally graded square plates ( $a/b = 1$ ,  $h/a = 0.1$ ).

$\alpha$	Present (CPT)	Present (FSDT)	Present (TSDT)	Ref [19]	Ref [23]	Diff with [19] (TSDT)
0	5.92483	5.79441	5.7694	5.7693	5.6763	0.001
0.5	5.14926	4.91874	4.9015	4.9207	4.8209	0.39
1	4.92899	4.91874	4.4192	4.4545	4.3474	0.79
2	4.71048	4.02911	4.0090	4.0063	3.9474	0.067
5	4.39092	3.80486	3.76823	3.7837	3.7218	0.41
8	4.16293	3.72511	3.6846	3.6830	3.6410	0.04
10	4.04527	3.67619	3.63684	3.6277	3.5928	0.25

**Table 5.** Comparison of the fundamental natural frequency parameters ( $\beta = \omega a^2 \sqrt{\rho_r h / D}$ ,  $\omega$ (Hz)) for a simply supported square isotropic plate in contact with fluid.

$b_1 / b$	Ref [11]	Present (CPT)	Present (FSDT)	Present (TSDT)	Diff (TSDT)
0	3.169	3.141	3.140	3.139	0.94
0.2	3.064	3.021	3.020	3.020	1.43
0.4	2.196	2.192	2.191	2.191	0.22
0.6	1.496	1.415	1.414	1.414	5.48
0.8	1.173	1.032	1.031	1.031	12.1
1	1.036	0.861	0.860	0.860	16.9

the rigid container walls. Calculations are performed using the commercial software, Mathematica (version 7), and the results are presented in tabular and graphical forms for different boundary conditions, plate parameters, and fluid parameters. In the present study, three different boundary conditions are investigated, namely; simply supported immovable (SSI), simply supported movable (SSM) and clamped (CL) edges. The presented results are obtained using a model with 33 dots.

### 6.1. The Effect of Plate Aspect Ratio ( $a/b$ ) on the Wet Natural Frequency

Fundamental wet natural frequencies of a functionally graded (AL/AL<sub>2</sub>O<sub>3</sub>) rectangular plate versus plate aspect ratio are illustrated in Fig. 3 for different boundary conditions. The results in Fig. 3 are shown for 40% fluid depth ratio and dimensions of  $b = 1$  m,  $h/a = 0.1$ ,  $b_1/b = 0.5$ , and  $c_1 = 0.4$  m while gradient index  $\alpha$  varies from 0 to 5. From Fig. 3, it is observed that the wet natural frequencies of the plates with SSI and SSM boundary conditions give exactly the same results. Moreover, it is observed that the highest values of fundamental wet natural frequency correspond to clamped boundary conditions.

### 6.2. The Effect of Fluid Depth on the Wet Natural Frequency

Fig. 4 illustrates fundamental wet natural frequencies of a functionally graded (AL/AL<sub>2</sub>O<sub>3</sub>) rectangular plate ( $a = 1$  m,  $b = 1$  m,  $h/a = 0.1$ ,  $c_1 = 0.4$  m,  $a/b = 1$ ) versus fluid depth for SSI and SSM and clamped boundary conditions while gradient index  $\alpha$  varies from 0 to 5. The wet natural frequencies of the functionally graded rectangular plate in contact with fluid are always less than the corresponding natural frequencies of the plate in air. Due to this fact, when normalizing the natural frequency with respect to the free plate natural frequencies, one can see that defined normalized natural frequencies of fluid-structure coupled system always lie between unity and zero. In Fig. 4, the results are shown for the plate partially in contact with water where the depth of the fluid ( $b_1/b$ ) varies from 0 to 0.9. From this figure, it is realized that the wet natural frequencies decrease as fluid depth increases.

### 6.3. The Effect of Plate Thickness Ratio ( $h/a$ ) on the Wet Natural Frequency

In Fig. 5, the influence of the thickness ratios on the fundamental wet natural frequencies is illustrated for a functionally graded (AL/AL<sub>2</sub>O<sub>3</sub>) rectangular plate ( $a = 1$  m,  $b = 1$  m,  $b_1/b = 1$ ,  $c_1 = 0.4$  m,  $a/b = 1$ ) with SSI and SSM boundary conditions while gradient index  $\alpha$  varies from 0 to 5. From Fig. 5, it is observed that the fundamental wet natural frequency of the plate increases monotonically, as the thickness ratio increases. This is not a surprising result since we know higher values of thickness ratio increase the stiffness of the structure more effectively than its inertia and thus, higher vibration frequencies are expected.

### 6.4. The Effect of Tank Width on the Wet Natural Frequency

Fig. 6 shows fundamental wet natural frequency of a functionally graded (AL/AL<sub>2</sub>O<sub>3</sub>) rectangular plate ( $a = 1$  m,  $b_1/b = 0.5$ ,  $h/a = 0.1$ ,  $a/b = 1$ ) versus fluid width. From these results, it is seen that the fundamental wet natural frequency increases as the tank width increases and approaches an asymptotic value. This means that for high enough values of width ratio, one can use the assumption of infinite fluid depth. In addition, Fig. 6 shows that width the wet natural frequencies corresponding to CL boundary conditions possess higher values for all values of fluid in comparison with SSI and SSM boundary conditions, which agree with the results of previous subsections.

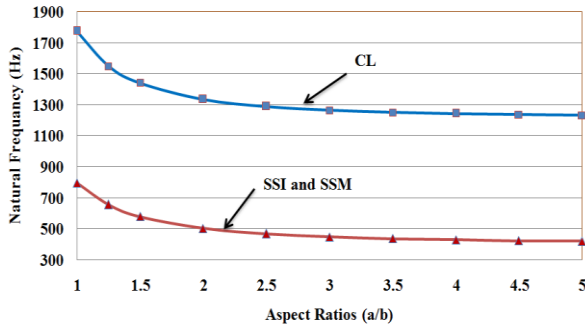


**Figure 3.** Variation of fundamental wet natural frequency of functionally graded (Al/Al<sub>2</sub>O<sub>3</sub>) rectangular plates versus aspect ratios for three combinations of boundary conditions using TSDT ( $c_1=0.4$  m,  $h/a=0.1$ ,  $b_1/b=0.4$ ,  $\alpha=2$ )

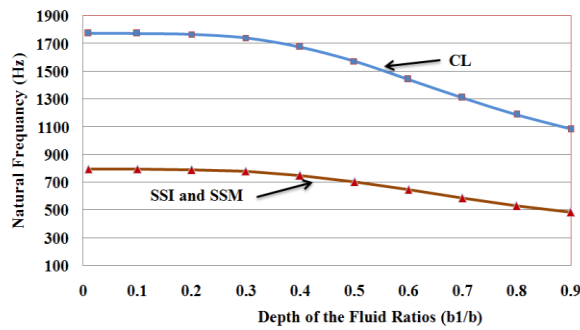


**Figure 4.** Variation of fundamental wet natural frequency versus depth of the fluid for a functionally graded (Al/Al<sub>2</sub>O<sub>3</sub>) rectangular with three combinations of boundary conditions using TSDT ( $c_1=0.4$  m,  $h/a=0.1$ ,  $a/b=1$ ,  $\alpha=2$ )

### 7. Conclusion

In this study hydrostatic vibration analysis of a functionally graded (AL/AL<sub>2</sub>O<sub>3</sub> and AL/ZrO<sub>2</sub>) rectangular plate partially in contact with a bounded fluid is investigated. For this purpose, Classical

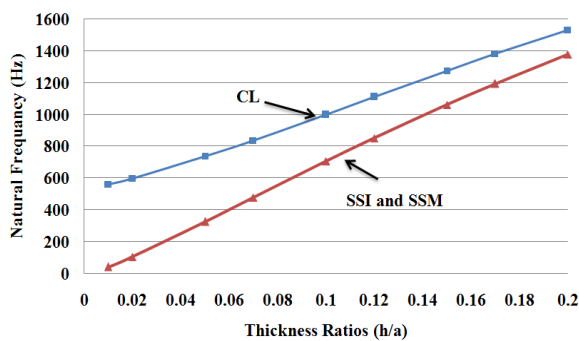


**Figure 5.** Variation of fundamental wet natural frequency versus thickness ratios for a functionally graded (Al/Al<sub>2</sub>O<sub>3</sub>) rectangular with three combinations of boundary conditions using TSDT ( $c_1=0.4$  m,  $a/b=1$ ,  $b_1/b=1$ ,  $\alpha=2$ )

(CPT), the First order Shear Deformation (FSDT) and the Third order Shear Deformation (TSDT) plate theories are employed. Using numerical data provided, the effect of different parameters including boundary conditions, material properties, aspect ratio, thickness ratio, and dimensions of the tank on the plate natural frequencies is examined and discussed in detail. The obtained results show that the accuracy of fundamental natural frequencies computed using CPT decreases as the thickness ratio increases. These results show that interaction between plate and fluid causes the wet mode shapes to distort from the dry mode shapes of the plate. Especially, severe distortions from dry modes are observed in the higher vibration modes. Also, it is observed that the mode shapes change according to the fluid depth and the wet natural frequencies decrease as fluid depth increases. The fundamental wet natural frequency of the plate increases monotonically as the thickness ratio increases. For all values of depth ratio and thickness ratio the frequencies corresponding to clamped boundary conditions possess higher values in comparison with movable and immovable simply supported boundary conditions. Numerical results reveal that the fundamental wet natural frequency increases as the tank width increases and approaches an asymptotic value. Moreover, the higher the aspect ratio is, the lower the natural frequencies are.

### Acknowledgements

The authors gratefully acknowledge the funding by Arak University, under grant No 91/9423.

### Appendix

#### APPENDIX A: Stress-Displacement Relationships

##### A-1. Classical Plate Theory (CPT)

Three independent displacements variables  $u$ ,  $v$  and  $w$ , in  $x$ ,  $y$  and  $z$  directions, respectively, are used to describe deformations of the plate; the geometric imperfection (or initial deformation due to hydrostatic pressure, Appendix C)  $w_0$  in normal direction is also introduced. The displacements  $u_1$ ,  $u_2$ ,  $u_3$  of a generic point of the plate at distance  $z$  from the  $z=0$  plane (see Figure 1) are related to the middle surface displacements  $u$ ,  $v$ ,  $w$  by:

$$u_1 = u - (z + h/2) \frac{\partial w}{\partial x} \tag{A 1}$$

$$u_2 = v - (z + h/2) \frac{\partial w}{\partial y} \tag{A 2}$$

$$u_3 = w + w_0 \tag{A 3}$$

The von Kàrmàn nonlinear strain–displacement relationships are introduced to describe the deformations of the plate. The strain components  $\varepsilon_x, \varepsilon_y$  and  $\gamma_{xy}$  at an arbitrary point of the plate are related to the middle surface strains  $\varepsilon_{x,0}, \varepsilon_{y,0}$  and  $\gamma_{xy,0}$  and the torsion of the middle surface  $k_x, k_y$  and  $k_{xy}$  by the following three relationships:

$$\varepsilon_x = \varepsilon_{x,0} + (z + h/2) k_x^{(0)} \quad (\text{A } 4)$$

$$\varepsilon_y = \varepsilon_{y,0} + (z + h/2) k_y^{(0)} \quad (\text{A } 5)$$

$$\gamma_{xy} = \gamma_{xy,0} + (z + h/2) k_{xy}^{(0)} \quad (\text{A } 6)$$

where

$$\varepsilon_{x,0} = \frac{\partial u}{\partial x} + \frac{\partial w}{\partial x} \frac{\partial w_0}{\partial x} \quad (\text{A } 7)$$

$$\varepsilon_{y,0} = \frac{\partial v}{\partial y} + \frac{\partial w}{\partial y} \frac{\partial w_0}{\partial y} \quad (\text{A } 8)$$

$$\gamma_{xy,0} = \frac{\partial u}{\partial y} + \frac{\partial v}{\partial x} + \frac{\partial w}{\partial x} \frac{\partial w_0}{\partial y} + \frac{\partial w_0}{\partial x} \frac{\partial w}{\partial y} \quad (\text{A } 9)$$

$$k_x^{(0)} = -\frac{\partial^2 w}{\partial x^2} \quad (\text{A } 10)$$

$$k_y^{(0)} = -\frac{\partial^2 w}{\partial y^2} \quad (\text{A } 11)$$

$$k_{xy}^{(0)} = -2 \frac{\partial^2 w}{\partial x \partial y} \quad (\text{A } 12)$$

### A-2. First-Order Shear Deformation Theory (FSDT)

Five independent variables, three displacements  $u, v, w$  and two rotations  $\phi_1$  and  $\phi_2$ , are used to describe the plate's middle plane deformation. This theory may be regarded as the thick-plate version of the von Kàrmàn theory.

The hypotheses are: (i) the transverse normal stress  $\sigma_z$  is negligible; in general, this is a good approximation of the actual behaviour of moderately thick plates; and (ii) the normal to the middle surface of the plate before deformation remains straight, but not necessarily normal, after deformation; this is a relaxed version of the Kirchhoff's hypothesis.

The displacements  $u_1, u_2, u_3$  of a generic point at distance  $z$  from the  $z=0$  plane (see Fig. 1) are related to the middle surface displacements  $u, v, w, \phi_1$  and  $\phi_2$  by the following equations:

$$u_1 = u + (z + h/2)\phi_1 \quad (\text{A } 13)$$

$$u_2 = v + (z + h/2)\phi_2 \quad (\text{A } 14)$$

$$u_3 = w + w_0 \quad (\text{A } 15)$$

where  $\phi_1$  and  $\phi_2$  are the rotations of the transverse normal about the  $y$  and  $x$  axes, respectively. A linear field in  $z$  is assumed for the first-order shear deformation theory. In Eq. (B-15) it is assumed that the normal displacement is constant through the thickness, which means  $\varepsilon_z = 0$ .

The strain-displacement equations for the first-order shear deformation theory are given by the following equations:

$$\varepsilon_x = \varepsilon_{x,0} + (z + h/2) k_x^{(0)} \quad (\text{A } 16)$$

$$\varepsilon_y = \varepsilon_{y,0} + (z + h/2) k_y^{(0)} \quad (\text{A } 17)$$

$$\gamma_{xy} = \gamma_{xy,0} + (z + h/2) k_{xy}^{(0)} \quad (\text{A } 18)$$

$$\gamma_{xz} = \gamma_{xz,0} \quad (\text{A } 19)$$

$$\gamma_{yz} = \gamma_{yz,0} \quad (\text{A } 20)$$

where

$$\varepsilon_{x,0} = \frac{\partial u}{\partial x} + \frac{\partial w}{\partial x} \frac{\partial w_0}{\partial x} \quad (\text{A } 21)$$

$$\varepsilon_{y,0} = \frac{\partial v}{\partial y} + \frac{\partial w}{\partial y} \frac{\partial w_0}{\partial y} \quad (\text{A } 22)$$

$$\gamma_{xy,0} = \frac{\partial u}{\partial y} + \frac{\partial v}{\partial x} + \frac{\partial w}{\partial x} \frac{\partial w_0}{\partial y} + \frac{\partial w_0}{\partial x} \frac{\partial w}{\partial y} \quad (\text{A } 23)$$

$$\gamma_{xz,0} = \phi_1 + \frac{\partial w}{\partial x} \quad (\text{A } 24)$$

$$\gamma_{yz,0} = \phi_2 + \frac{\partial w}{\partial y} \quad (\text{A } 25)$$

$$k_x^{(0)} = \frac{\partial \phi_1}{\partial x} \quad (\text{A } 26)$$

$$k_y^{(0)} = \frac{\partial \phi_2}{\partial y} \quad (\text{A } 27)$$

$$k_{xy}^{(0)} = \frac{\partial \phi_1}{\partial y} + \frac{\partial \phi_2}{\partial x} \quad (\text{A } 28)$$

$$\gamma_{yz} = \gamma_{yz,0} \quad (\text{A } 29)$$

Eqs. (A 19) and (A 20) show a uniform distribution of shear strains through the shell thickness, which gives uniform shear stresses. The actual distribution of shear stresses is close to a parabolic distribution through the thickness, taking zero value at the top and bottom surfaces. For this reason, for equilibrium considerations, it is necessary to introduce a shear correction factor with the first-order shear deformation theory in order not to overestimate the shear forces.

### A-3. Third-Order Shear Deformation Theory (TSDT)

A third-order shear deformation theory of plates is introduced by Reddy. The displacements of a generic point of the plate are related to the middle plane displacements by the following equations:

$$u_1 = u + (z + h/2)\phi_1 - \frac{4}{3h^2}(z + h/2)^3 \left( \phi_1 + \frac{\partial w}{\partial x} \right) \quad (\text{A 30})$$

$$u_2 = v + (z + h/2)\phi_2 - \frac{4}{3h^2}(z + h/2)^3 \left( \phi_2 + \frac{\partial w}{\partial y} \right) \quad (\text{A 31})$$

$$u_3 = w + w_0 \quad (\text{A 32})$$

where  $\phi_1$  and  $\phi_2$  are the rotations of the transverse normal at middle plan about the  $y$  and  $x$  axes, respectively, and the other terms can be computed as functions of  $w$ ,  $\phi_1$  and  $\phi_2$ . Eqs. (A 30) and (A 31) represent the parabolic distribution of shear effects through the thickness and satisfy the zero shear boundary condition at both the top and bottom surfaces of the plate.

The strain-displacement equations, keeping terms up to  $z^3$ , are written as follows:

$$\varepsilon_x = \varepsilon_{x,0} + (z + h/2) \left( k_x^{(0)} + (z + h/2)^2 k_x^{(2)} \right) \quad (\text{A 33})$$

$$\varepsilon_y = \varepsilon_{y,0} + (z + h/2) \left( k_y^{(0)} + (z + h/2)^2 k_y^{(2)} \right) \quad (\text{A 34})$$

$$\gamma_{xy} = \gamma_{xy,0} + (z + h/2) \left( k_{xy}^{(0)} + (z + h/2)^2 k_{xy}^{(2)} \right) \quad (\text{A 35})$$

$$\gamma_{xz} = \gamma_{xz,0} + (z + h/2) \left( (z + h/2) k_{xz}^{(1)} \right) \quad (\text{A 36})$$

$$\gamma_{yz} = \gamma_{yz,0} + (z + h/2) \left( (z + h/2) k_{yz}^{(1)} \right) \quad (\text{A 37})$$

where

$$\varepsilon_{x,0} = \frac{\partial u}{\partial x} + \frac{\partial w}{\partial x} \frac{\partial w_0}{\partial x} \quad (\text{A 38})$$

$$\varepsilon_{y,0} = \frac{\partial v}{\partial y} + \frac{\partial w}{\partial y} \frac{\partial w_0}{\partial y} \quad (\text{A 39})$$

$$\gamma_{xy,0} = \frac{\partial u}{\partial y} + \frac{\partial v}{\partial x} + \frac{\partial w}{\partial x} \frac{\partial w_0}{\partial y} + \frac{\partial w_0}{\partial x} \frac{\partial w}{\partial y} \quad (\text{A 40})$$

$$\gamma_{xz,0} = \phi_1 + \frac{\partial w}{\partial x} \quad (\text{A 41})$$

$$\gamma_{yz,0} = \phi_2 + \frac{\partial w}{\partial y} \quad (\text{A 42})$$

$$k_x^{(0)} = \frac{\partial \phi_1}{\partial x} \quad (\text{A 43})$$

$$k_y^{(0)} = \frac{\partial \phi_2}{\partial y} \quad (\text{A 44})$$

$$k_{xy}^{(0)} = \frac{\partial \phi_1}{\partial y} + \frac{\partial \phi_2}{\partial x} \quad (\text{A 45})$$

$$k_x^{(2)} = -\frac{4}{3h^2} \left( \frac{\partial \phi_1}{\partial x} + \frac{\partial^2 w}{\partial x^2} \right) \quad (\text{A 46})$$

$$k_y^{(2)} = -\frac{4}{3h^2} \left( \frac{\partial \phi_2}{\partial y} + \frac{\partial^2 w}{\partial y^2} \right) \quad (\text{A 47})$$

$$k_{xy}^{(2)} = -\frac{4}{3h^2} \left( \frac{\partial \phi_1}{\partial y} + \frac{\partial \phi_2}{\partial x} + 2 \frac{\partial^2 w}{\partial x \partial y} \right) \quad (\text{A 48})$$

$$k_{xz}^{(1)} = -\frac{4}{h^2} \gamma_{xz,0} \quad (\text{A 49})$$

$$k_{yz}^{(1)} = -\frac{4}{h^2} \gamma_{yz,0} \quad (\text{A 50})$$

### APPENDIX B: Boundary Conditions and Discretization [27]

The boundary conditions for simply supported plates with movable edges (SSM) are as the following:

$$v = w = \phi_2 = N_x = M_x = 0, \quad \text{at } x = 0, a, \quad (\text{B 1-5})$$

$$u = w = \phi_1 = N_y = M_y = 0, \quad \text{at } y = 0, b, \quad (\text{B 6-10})$$

Where  $N_x$  or  $N_y$  and  $M_x$  or  $M_y$  are the normal force and the bending moment per unit length, respectively.

The boundary conditions for simply supported plates with immovable edges (SSI) are as follows:

$$u = v = w = \phi_2 = M_x = 0, \quad \text{at } x = 0, a, \quad (\text{B 11-15})$$

$$u = v = w = \phi_1 = M_y = 0, \quad \text{at } y = 0, b. \quad (\text{B 16-20})$$

The boundary conditions for clamped plates (CL) are as follows:

$$u = v = w = \phi_1 = \phi_2 = 0, \quad \text{at } x = 0, a, \quad \text{and at } y = 0, b \quad (\text{B 21-25})$$

Three expansions of plate displacements are used to discretize the system for the different boundary conditions. For simply supported movable (SSM) edges, the displacements  $u$ ,  $v$  and  $w$  and rotations  $\phi_1$  and  $\phi_2$  are expanded using the following expressions, which satisfy identically the geometric boundary conditions:

$$\begin{aligned}
u(x, y, t) &= \sum_{m=1}^M \sum_{n=1}^N u_{m,n}(t) \cos\left(\frac{m\pi x}{a}\right) \sin\left(\frac{n\pi y}{b}\right) \\
v(x, y, t) &= \sum_{m=1}^M \sum_{n=1}^N v_{m,n}(t) \sin\left(\frac{m\pi x}{a}\right) \cos\left(\frac{n\pi y}{b}\right) \\
w(x, y, t) &= \sum_{m=1}^M \sum_{n=1}^N w_{m,n}(t) \sin\left(\frac{m\pi x}{a}\right) \sin\left(\frac{n\pi y}{b}\right) \quad (\text{B 26-30}) \\
\phi_1(x, y, t) &= \sum_{m=1}^M \sum_{n=1}^N \phi_{1m,n}(t) \cos\left(\frac{m\pi x}{a}\right) \sin\left(\frac{n\pi y}{b}\right) \\
\phi_2(x, y, t) &= \sum_{m=1}^M \sum_{n=1}^N \phi_{2m,n}(t) \sin\left(\frac{m\pi x}{a}\right) \cos\left(\frac{n\pi y}{b}\right)
\end{aligned}$$

where  $m$  and  $n$  are the numbers of half-waves in  $x$  and  $y$  directions, respectively, and  $t$  is the time;  $u_{m,n}(t)$ ,  $v_{m,n}(t)$ ,  $w_{m,n}(t)$ ,  $\phi_{1m,n}(t)$  and  $\phi_{2m,n}(t)$  are the generalized coordinates, which are unknown functions of  $t$ .  $M$  and  $N$  indicate the terms necessary in the expansion of the in-plane displacements and, in general, are larger than  $\hat{M}$  and  $\hat{N}$ , respectively, which indicate the terms in the expansion of out-of-plane displacement and rotations.

For simply supported immovable (SSI) edges, the following expansions are used:

$$\begin{aligned}
u(x, y, t) &= \sum_{m=1}^M \sum_{n=1}^N u_{m,n}(t) \sin\left(\frac{2m\pi x}{a}\right) \sin\left(\frac{n\pi y}{b}\right) \\
v(x, y, t) &= \sum_{m=1}^M \sum_{n=1}^N v_{m,n}(t) \sin\left(\frac{m\pi x}{a}\right) \sin\left(\frac{2n\pi y}{b}\right) \\
w(x, y, t) &= \sum_{m=1}^M \sum_{n=1}^N w_{m,n}(t) \sin\left(\frac{m\pi x}{a}\right) \sin\left(\frac{n\pi y}{b}\right) \quad (\text{B 31-35}) \\
\phi_1(x, y, t) &= \sum_{m=1}^M \sum_{n=1}^N \phi_{1m,n}(t) \cos\left(\frac{m\pi x}{a}\right) \sin\left(\frac{n\pi y}{b}\right) \\
\phi_2(x, y, t) &= \sum_{m=1}^M \sum_{n=1}^N \phi_{2m,n}(t) \sin\left(\frac{m\pi x}{a}\right) \cos\left(\frac{n\pi y}{b}\right)
\end{aligned}$$

Finally, for clamped edges (CL), the expansions take the following form:

$$\begin{aligned}
u(x, y, t) &= \sum_{m=1}^M \sum_{n=1}^N u_{m,n}(t) \sin\left(\frac{2m\pi x}{a}\right) \sin\left(\frac{n\pi y}{b}\right) \\
v(x, y, t) &= \sum_{m=1}^M \sum_{n=1}^N v_{m,n}(t) \sin\left(\frac{m\pi x}{a}\right) \sin\left(\frac{2n\pi y}{b}\right) \\
w(x, y, t) &= \sum_{m=1}^M \sum_{n=1}^N w_{m,n}(t) \sin\left(\frac{m\pi x}{a}\right) \sin\left(\frac{n\pi y}{b}\right) \quad (\text{B 36-40}) \\
\phi_1(x, y, t) &= \sum_{m=1}^M \sum_{n=1}^N \phi_{1m,n}(t) \sin\left(\frac{m\pi x}{a}\right) \sin\left(\frac{n\pi y}{b}\right) \\
\phi_2(x, y, t) &= \sum_{m=1}^M \sum_{n=1}^N \phi_{2m,n}(t) \sin\left(\frac{m\pi x}{a}\right) \sin\left(\frac{n\pi y}{b}\right)
\end{aligned}$$

### APPENDIX C: The Effect of the Hydrostatic Triangular Pressure

To account the effect of the hydrostatic triangular pressure, the virtual work corresponding to the hydrostatic triangular pressure is estimated by the following equation:

$$U_h = \frac{1}{2} \rho_F g \int_0^a \int_0^{b_1} w(b_1 - y) dy dx, \quad (\text{C 1})$$

The virtual work due to hydrostatic triangular pressure can be taken into account for the forced and nonlinear vibrations. In order to take into account the effects of hydrostatic triangular pressure on the linear free vibration, the plate configuration due to hydrostatic triangular pressure is developed. The plate configuration for the thin plates due to hydrostatic triangular pressure is approximated as follows:

$$w_0 = \sum_{m=1}^{\infty} \sum_{n=1}^{\infty} A_{hp}(m, n) \sin(m\pi x / a) \sin(n\pi y / b) \quad (\text{C 2})$$

where  $A_{hp}$  is the unknown constant coefficient. Applying bi-harmonic equation  $\nabla^4 w_0 = -\rho_F g (b_1 - y)$  coefficient  $A_{hp}$  is defined as follows:

$$A_{hp}(m, n) \pi^4 ((m/a)^2 + (n/b)^2)^2 \times \sin(m\pi x / a) \sin(n\pi y / b) = -\rho_F g (b_1 - y) \quad (\text{C 3})$$

From Eq. (A-3), the associated Fourier coefficient  $A_{hp}$  is obtained as follows:

$$A_{hp}(m, n) = \frac{1}{ab_1} \int_0^a \int_0^{b_1} \rho_F g (b_1 - y) \sin\left(\frac{m\pi x}{a}\right) \sin\left(\frac{n\pi y}{b}\right) dy dx \quad (C 4)$$

$$- \frac{\pi^4 ((m/a)^2 + (n/b)^2)^2}{\pi^4 ((m/a)^2 + (n/b)^2)^2}$$

The system is then studied in the case of a plate contacting water on both sides. In this case, the contribution of the initial deformation of the plate, given by the hydrostatic pressure of the fluid, can be eliminated if the water level in both tanks is identical.

## References

- [1] Khorshidi K. Effect of Hydrostatic Pressure on Vibrating Rectangular Plates Coupled with Fluid. *Scientia Iranica: Transaction A: Civil Engineering* 2010; 17(6): 415-429.
- [2] Amabili M. Eigenvalue problems for vibrating structures coupled with quiescent fluids with free surface. *Sound Vib* 2000; 231(1): 79-97.
- [3] JeongKH., Kim JW. Hydrostatic vibration analysis of two flexible rectangular plates partially coupled with liquid. *Nuclear Eng Technol* 2009; 41(3): 335-345.
- [4] Jeong KH, Lee GM, Kim TW, Park KB. Free Vibration of a rectangular plate partially in contact with a liquid at both sides. *The Korea Society Noise Vib Eng* 2008; 18(1): 123-130 (In Korean).
- [5] Jeong KH, Yoo GH, Lee SC. Hydroelastic vibration of two identical rectangular plates. *Sound Vib* 2003; 272: 539-555.
- [6] Kwak MK. Hydroelastic vibration of rectangular plates. *Transaction of the American Society of Mechanical Engineers, Appl Mech* 1996; 63: 110-115.
- [7] Zhou D, Cheung YK. Vibration of vertical rectangular plate in contact with water on one side. *Earthq Eng Struct D* 2000; 29: 693-710.
- [8] Chang TP, Liu MF. On the natural frequency of a rectangular isotropic plate in contact with fluid. *J Sound Vib* 2000; 236: 547-553.
- [9] Ergin A, Uğurlu B. Linear vibration analysis of cantilever plates partially submerged in fluid. *Fluids Struct* 2003; 17: 927-939.
- [10] Zhou D, Liu W. Hydroelastic vibrations of flexible rectangular tanks partially filled with fluid. *Int J Numer Methods Eng* 2007; 71: 149-174.
- [11] Uğurlu B, Kutlu A, Ergin A, Omurtag MH. Dynamics of a rectangular plate resting on an elastic foundation and partially in contact with a quiescent fluid. *Sound Vib* 2008; 317: 308-328.
- [12] Kerboua Y, Lakis AA, Thomas M, Marcouiller L. Vibration analysis of rectangular plates coupled with fluid. *Appl Math Modeling* 200; 32: 2570-2586.
- [13] Abrate S., Functionally graded plates behave like homogeneous plates, *Compos Part B-Eng* 2008; 39: 151-158.
- [14] Zhang DG, Zhou YH. A theoretical analysis of FGM thin plates based on physical neutral surface. *Comp Mater Sci* 2008; 44: 716-720.
- [15] Woo J, Meguid SA, Ong LS. Nonlinear free vibration behavior of functionally graded plates. *Sound Vib* 2006; 289: 595-611.
- [16] Reddy JN, Cheng ZQ. Frequency of functionally graded plates with three-dimensional asymptotic approach. *Eng Mech ASCE* 2003; 129: 896-900.
- [17] Qian LF, Batra RC, Chen LM. Static and dynamic deformations of thick functionally graded elastic plate by using higher-order shear and normal deformable plate theory and meshless local Petrov-Galerkin method. *Compos Part B-Eng* 2004; 35: 685-697.
- [18] Vel SS, Batra RC. Three-dimensional exact solution for the vibration of functionally graded rectangular plates. *sound Vib* 2004; 272: 703-730.
- [19] Hosseini-Hashemi Sh, Rokni Damavandi Taher H, Akhavan H, Omidi M. Free vibration of Functionally graded rectangular plates use first-order shear deformation plate theory. *Appl Math Modelling* 2010; 34: 1276-1291.
- [20] Hosseini-Hashemi Sh, Rokni Damavandi Taher H, Akhavan H, Omidi M. study on the free vibration of thick functionally graded rectangular plates according to the new exact closed-form procedure. *Comp Struct* 2011; 93: 722-735.
- [21] Suresh Kumar J, Sidda Reddy B, Eswara Reddy C, Vijaya Kumar Reddy K. Higher order theory for free vibration analysis of functionally graded material plates. *ARNP J EngApplSci* 2011; 6(10): 105-111.
- [22] Jha DK, Kant T, Singh RK. Higher order shear and normal deformation theory for natural frequency of functionally graded rectangular plates. *Nuclear Eng and Design* 2012; 250: 8-13.
- [23] Zhao X, Lee YY, Liew KM. Free vibration analysis of functionally graded plates using the element-free kp- Ritz method. *sound Vib* 2009; 319: 918-939.
- [24] Huang CS, McGee OG, Chang MJ. Vibrations of cracked rectangular FGM thick plates. *Comp Struct* 2011; 93: 1747-1764.
- [25] Thai HT, Choi DH. A refined shear deformation theory for free vibration of functionally graded plates on elastic foundation. *Comp Part B* 2012; 43: 2335-2347.

- [26] Zhu P, Liew KM. Free vibration analysis of moderately thick functionally graded plates by local Krigingmeshless method. *Comp Struct* 2011; 93: 2925–2944.
- [27] Khorshidi K, Farhadi S. Free Vibration Analysis of a Laminated Composite Rectangular Plate in Contact with a Bounded Fluid. *Comp Struct* 2013; 104: 176–186.
- [28] Bishop RED. *The Mechanics of Vibration*. Cambridge University Press, New York, 1979.